RESEARCH ARTICLE
ATMOSPHERIC PHYSICS

Earth and Planetary Physics
8: 415–422, 2024
doi: 10.26464/epp2024007

Analysis of gravity wave activity during stratospheric sudden warmings in the northern hemisphere

XuanYun Zeng[1,2*], and Guang Zhong[1]

[1]School of Physics and Electronic Sciences, Changsha University of Science and Technology, Changsha 410000, China;

[2]Key Laboratory of Geospace Environment, Chinese Academy of Sciences, University of Science & Technology of China, Hefei 230026, China

Key Points:

- During stratospheric sudden warming (SSW) periods, the stratospheric temperature was found to be enhanced in one or two longitudinal regions; the areas affected extended to the east of 90°W.
- During SSWs, gravity waves (GWs) exhibited regions of enhanced E_p; these regions expanded eastward and downward compared to their pre-SSW extension.
- The GWs' E_p was partially filtered by the eastward zonal winds, and increased when zonal winds weakened or turned westward.

Citation: Zeng, X. Y., and Zhong, G. (2024). Analysis of gravity wave activity during stratospheric sudden warmings in the northern hemisphere. *Earth Planet. Phys.*, *8*(2), 415–422. http://doi.org/10.26464/epp2024007

Abstract: Due to the significant changes they bring to high latitude stratospheric temperature and wind, stratospheric sudden warmings (SSWs) can have an impact on the propagation and energy distribution of gravity waves (GWs). The variation characteristics of GWs during SSWs have always been an important issue. Using temperature data from January to March in 2014–2016, provided by the Constellation Observing System for Meteorology, Ionosphere and Climate (COSMIC) mission, we have analyzed global GW activity at 15–40 km in the Northern Hemisphere during SSW events. During the SSWs that we studied, the stratospheric temperature rose in one or two longitudinal regions in the Northern Hemisphere; the areas affected extended to the east of 90°W. During these SSWs, the potential energy density (E_p) of GWs expanded and covered a larger range of longitude and altitude, exhibiting an eastward and downward extension. The E_p usually increased, while partially filtered by the eastward zonal winds. When zonal winds weakened or turned westward, E_p began to strengthen. After SSWs, the E_p usually decreased. These observations can serve as a reference for analyzing the interaction mechanism between SSWs and GWs in future work.

Keywords: stratospheric sudden warming; gravity wave; wind filter

1. Introduction

Gravity waves (GWs) are one of the common disturbances in the middle and upper atmosphere; they play a vital role in atmospheric motion (Fritts and Alexander, 2003; Chang SJ et al., 2020; TengChen KM et al., 2021; Yi W et al., 2023a). They are an important factor affecting changes in stratospheric wind and temperature fields. The breaking of upward propagating GWs is the main source of small-scale turbulence and mixing in the middle and upper atmosphere (He Y et al., 2020a). The momentum flux caused by the generation, propagation, and breaking of GWs affects atmospheric circulation (Bian JC et al., 2005; Li T et al., 2007; Gu SY et al., 2020; Ji QQ et al., 2022; Yi W et al., 2021, 2023b).

In recent years, GWs have been studied using different instruments and methods, such as ground-based radar observation, observation from meteorological rockets, radiosonde and satellite observation, and the application of deep learning (Xiao CY and Hu X, 2010; Chang SJ et al., 2019; He Y et al., 2020b, 2020c; Xue XH et al., 2020; He Y et al., 2021, 2022a, 2023; Wu Y et al., 2022; Zhang J et al., 2023). Satellite observation is superior to ground observation because the area measured by a satellite is often larger than can be observed by ground instruments, and some satellite observations also provide better temporal and vertical resolution than ground-based systems (Jin S and Feng GP, 2011; Jin S et al., 2013). A large number of satellite-mounted instruments have been used to observe temporal and spatial distribution characteristics of GWs (Wu DL and Waters, 2013; He Y et al, 2022b; Ge W et al., 2023). The distribution characteristics of global GW activity have been studied, and the impact of background wind field on GWs has been discussed (Tsuda et al., 2016; Jia MJ et al., 2018; Wu JF et al., 2018; Ge W et al., 2019; Yi W et al., 2019; He Y et al., 2020d; Ern et al., 2022). Although results obtained by data from these satellites are sufficiently detailed, there are still deficiencies, such as low spatial resolution and low data density, leading to limited knowledge of spatial distribution and temporal variation of GWs. The Constellation Observing System for Meteorology, Ionosphere and Climate (COSMIC) mission provides data with global coverage and high vertical and temporal resolution. Therefore, COSMIC

Correspondence to: X. Y. Zeng, zengxy@csust.edu.cn
Received 28 OCT 2023; Accepted 17 DEC 2023.
First Published online 31 JAN 2024.

data are particularly suitable for studying the activities of global GWs (Wang L and Alexander, 2009; Wright et al., 2011; Mcdonald, 2012).

Stratospheric sudden warming (SSW) is a phenomenon that occurs in the polar regions of the winter hemisphere. Normally, the temperature in the winter hemisphere's stratosphere gradually decreases as the latitude increases, and the zonal mean zonal winds in the polar stratosphere are eastward. However, in certain winters, the state of polar regions is severely disturbed. The temperature of the polar stratosphere can increase rapidly in a short period of time; at an altitude of 10 hPa near the pole, the temperature can rise by 40–60 K within a week. As the temperature rises, the eastward polar vortex is weakened, and winds even reverse from eastward to westward (Harvey et al., 2002).

The SSW phenomenon was discovered by German scientist Richard Scherhag in 1952 when analyzing radiosonde data (Scherhag, 1952). Radiosonde observations provided useful data on the troposphere and stratosphere during SSW events. Later, probe rocket observations added data that extended to the height of the mesosphere. Today, satellite observation data provide ideal spatiotemporal coverage, making it possible to study the global impact of SSW events (Zhou B et al., 2023).

Recent observations and theoretical investigations have shown that the effects of SSW events are global (Laskar et al., 2019; Kogure et al., 2021; Watanabe et al., 2022). SSWs can not only alter the temperature structure of the polar atmosphere and the polar night jet, but can also alter the meridional circulation, thereby affecting mid to low latitudes (Laskar et al., 2019). The climatology of stratospheric polar vortices and anticyclones has been investigated (Harvey et al., 2002). Therefore, studying changes in atmospheric parameters on a global scale during SSW events can help us understand the dynamic processes of the atmosphere.

The SSW is a dynamical phenomenon of the wintertime stratosphere, caused by interaction between the stratospheric zonal-mean flow and planetary rossby waves propagating from the troposphere. There are two different types of such warmings, identified as the vortex *displacement type* (dominant wave number is 1, i.e. wavenumber 1 [WN1]), and the vortex *splitting type* (dominant wave number is 2, i.e. wavenumber 2 [WN2]) (Charlton and Polvani, 2007; Seviour et al., 2013; Butler and Domeisen, 2021). The occurrence of an SSW is mainly due to interaction in winter between enhanced planetary waves (PWs) and the atmospheric background mean flow. SSWs are very common in the northern hemisphere, where PWs are enhanced by the interaction between sea and land; in the southern hemisphere, where middle and high latitudes are mostly oceanic, lack of sea–land interactions results in many fewer PWs and SSWs. The rapid changes of temperature and wind in the upper and middle atmosphere of the winter hemisphere that characterize an SSW have significant impact on the atmospheric circulation (Tang L et al., 2023). During SSWs, the temperature of the polar stratosphere increases rapidly — within a few days, accompanied by weakenings of the polar vortex and easterly winds. The breaking of polar vortex and the reverse of winds happen even during the main warming period. In high latitudes, the main dissipation region of GWs is above the stratosphere. Due to the significant changes they make in the background atmosphere of the high latitude stratosphere over a short period of time, SSWs can significantly affect the propagation and energy distribution of GWs. Reduced GW activity was observed during the 2009 major SSW event (Kalisch and Chun HY, 2021). During the September 2019 SSW event in the Southern Hemisphere, strongly negative vertical fluxes of zonal momentum in the stratosphere were observed around the edge of the polar vortex (Minamihara et al., 2022). Positive feedback between GW forcing and the state of the polar vortex has been discussed (Wicker et al., 2023); they report that the associated polar stratospheric cold bias following SSW events in sub-seasonal hindcasts can be halved by increasing vertical model resolution, suggesting a potential sensitivity to GW forcing. PWs are considered the main driving force of SSWs. However, theoretical studies have suggested that GWs can interact with background circulation and contribute to the occurrences of SSWs (Cullens and Thurairajah, 2021). More work is needed to study the characteristics of GW activities during SSWs to help elucidate the interaction mechanisms between SSWs and GWs.

The purpose of this study is to use COSMIC radio occultation (RO) temperature data to analyze the characteristics of GW activity in the Northern Hemisphere during SSWs. The results can serve as a reference for future work studying interaction mechanisms between SSWs and GWs.

2. Data and Methods

The COSMIC mission was launched on April 15, 2006. It consists of six low-earth-orbit satellites with an inclination of about 72° and an interval of about 30°. Radio occultation (RO) occurs when tracking occludes global positioning system (GPS) satellites above or below the earth's horizon. Theoretically, COSMIC can obtain about 3000 RO profiles every day, but some profiles cannot obtain reasonable atmospheric physical quantities; roughly 2000 profiles a day can be used to calculate temperature data. COSMIC observation data are sufficient to achieve global, all-weather coverage with high vertical resolution.

We selected dry temperature profiles of COSMIC RO level 2 data collected from January to March in 2014–2016. The GW activity is evaluated by the potential energy density (E_p) calculated from each profile. The altitude resolution of COSMIC temperature profile data is a few tenths of 1 km. Therefore, to achieve temperature profiles at altitude intervals of 0.1 km, we have interpolated temperatures from COSMIC data as needed. We extract GW disturbances as follows:

(1) within each latitude interval of 5°, daily temperature profiles are arranged by increasing longitude;

(2) least squares harmonic fitting is performed at each altitude (Zeng XY et al., 2017; Zeng XY et al., 2021) with a zonal wavenumber of 0–6, to obtain background temperature and large-scale fluctuations with zonal wavenumber of 1–6;

(3) background and large-scale fluctuations are subtracted from the original temperature to obtain the temperature residual;

(4) a sixth-order Butterworth bandpass filter with band width of 3–10 km is used to filter out large-scale vertical wavelength fluctuations, so as to obtain GW disturbance;

(5) the obtained GW disturbance is used to calculate the E_p.

The steps above allow interference of tides or PWs to be basically eliminated from the E_p calculation.

E_p is calculated as follows:

$$N^2(z) = \frac{g}{\overline{T}}\left(\frac{\partial \overline{T}}{\partial z} + \frac{g}{c_p}\right),$$

$$E_p = \frac{1}{2}\cdot\left(\frac{g}{N}\right)^2\cdot\left(\frac{\hat{T}}{\overline{T}}\right)^2,$$

where g is the acceleration due to gravity, $\overline{T}$ is the background temperature, z is the altitude, c_p is the isobaric heat capacity, N is the Brunt–Väisälä frequency, and $\hat{T}$ is the temperature amplitude.

The zonal wind distribution during SSWs has also been considered, using data provided by The European Centre for Medium-range Weather Forecast (ECMWF), which are re-analyses of observations.

3. Results and Discussion

We focus our research in the mid to high latitudes of the Northern Hemisphere in the first three months of 2014–2016, the season when SSWs usually occur (Manney et al., 2015; Gong Y et al., 2018; Ma Z et al., 2020a; Idolor et al., 2021), and analyze the temporal and spatial distribution of temperature and GW E_p. To create a grid to display temperature and E_p values, we divided the global projection into a grid by longitude × latitude × altitude × day (with intervals of 10° × 5° × 0.1 km × 1 day). Temperature and E_p profile data within each grid interval were identified and averaged to arrive at values for that interval. Here are the results.

3.1 The Temperature Variation during SSWs

Figure 1 shows the distribution of temperature at the altitude interval of 20–30 km between 30°N and 90°N latitude from January to March of the three years 2014 to 2016, as seen looking down from above the North Pole. Significant SSW events occurred each year in those months. From the perspective of the Northern Hemisphere, high-temperature and low-temperature regions alternated when SSWs began. Between days of the year (DOY) 040 to 052 in 2014, when an SSW event occurred (Idolor et al., 2021), temperature increased near 60°W–120°W. The other warming occurred near 60°E on DOYs 004–020 in 2015, and near 180°E DOY 036–040 in 2016, when SSW events also happened (Manney et al., 2015; Gong Y et al., 2018). We can see an interesting phenomenon that the area of high temperatures expanded to cover the polar region on DOY 40 in 2014 and DOY 004 in 2015. Besides, late in March of 2014 and 2016, the temperature in the

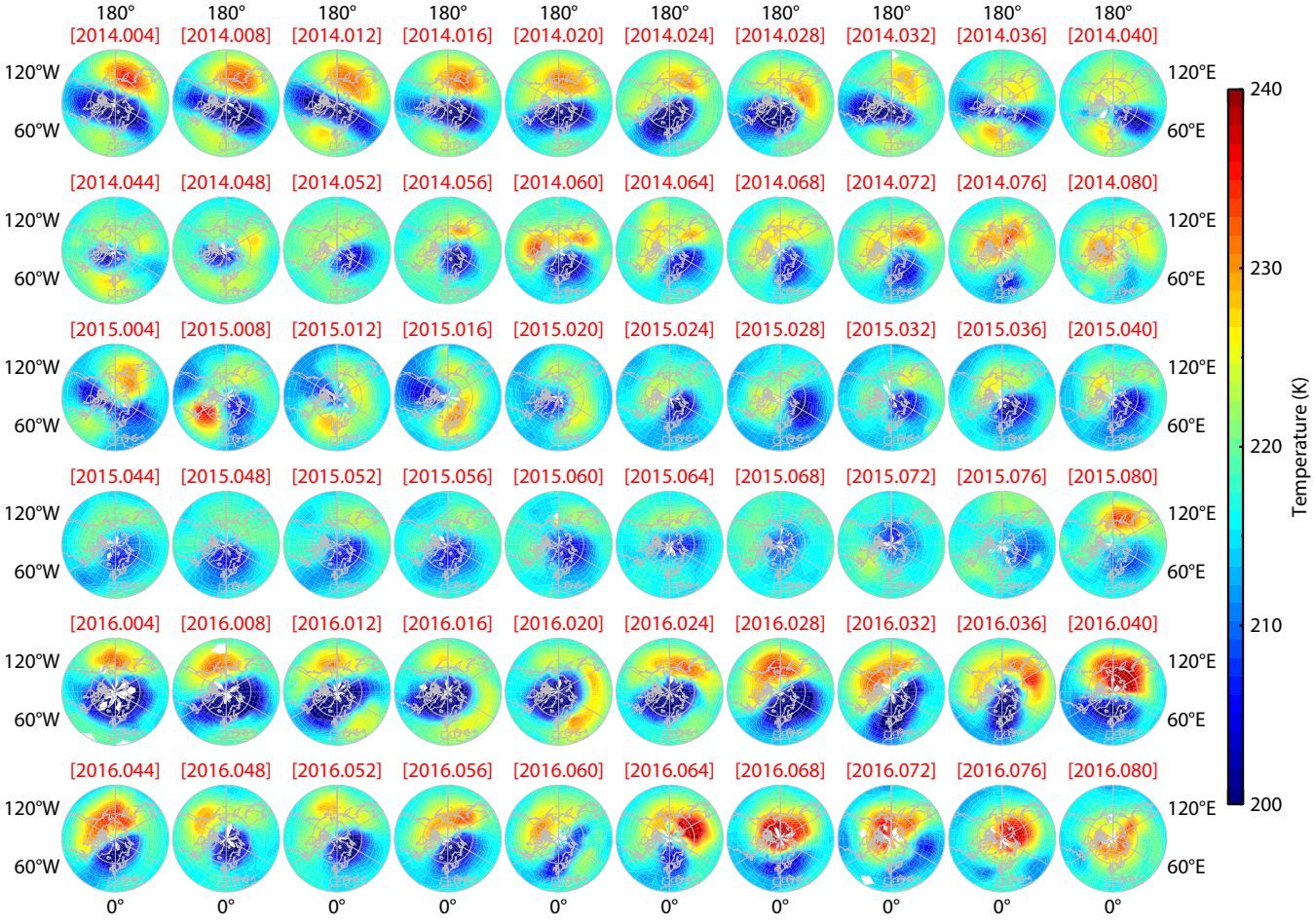

Figure 1. Images, overlooking the North Pole, show distribution of temperature, from 30°N to 90°N latitude, between January and March in the three years 2014–2016. Longitude is 180° at the top to 0° at the bottom of each image. Each temperature distribution image is labeled by year and day of the year.

mid to high altitude areas of the entire Northern Hemisphere increased.

The images in Figure 1 show temperature distribution characteristics during the first three months of 2014 to 2016, when SSWs frequently occurred. In the pre-warming period (before the onset or central date of an SSW), the temperature structure can indicate a dominant wave component (e.g., waves 1 or 2). In the post-warming period of an SSW, high temperatures can be transported to another hemisphere (e.g., from 120°E to 60°W) via the polar region, showing temperature enhancements in two longitudinal regions. This longitudinal dependence is caused by the anticyclones (Ma Z et al., 2020a). The average temperature in the mid to high altitude areas of the entire Northern Hemisphere increased late in March of 2014 and 2016. Those are stratospheric final warmings without a recovering of zonal mean zonal winds (Yamazaki et al., 2019). Final warmings in 2014–2016 are related to wave 1 (Butler and Domeisen, 2021). As a consequence, each year there was only one high temperature zone during final warmings.

3.2 Vertical Propagation of GWs during SSWs

To understand the variation of GW activities during SSWs, we first analyzed the vertical propagation of GWs. Figure 2 shows the longitude-altitude distribution of temperature (colored contour map) and GW E_p (the red line marks the value E_p = 3 J/kg) in the Northern Hemisphere from January to March in 2014–2016. We can see that when SSWs occurred, obvious enhancements of GW E_p were observed. The enhancement of GW E_p has an eastward and downward extension. We can see that during the period of SSWs in 2014–2016 mentioned in Section 3.1, the enhanced area of GW E_p expanded and covered a larger range of longitude and altitude. The altitudes at which E_p values exceeded 3 J/kg expanded down to below 20 km. The vertical propagation of GWs proved to be significant, which may have been caused by the GW sources and the wind field (Cullens and Thurairajah, 2021).

3.3 The Longitude and Latitude Distribution of GWs

In addition to the vertical variation, the horizontal spatial variation of GWs is also significant. Figure 3 shows the longitude-latitude distribution of temperature and GW E_p within 20–30 km at 30°N–90°N from January to March in 2014–2016. GW E_p values are drawn as a gray contour map. The temperature values of 205, 210, 220, 225 K are marked as the purple, blue, orange, and red lines. During the period of SSWs in 2014–2016 mentioned in Section 3.1, enhanced areas of GW E_p are shown to expand and cover a larger range of longitude and latitude. Usually, GWs are enhanced at the junction of high (marked by the red line) and low (marked by the blue line) temperature zones, sometimes slightly closer to the high temperature zone. The possible reason is that the area locates at the edge of the polar vortex where the background wind was strong, and the GWs were enhanced (Jia Y et al., 2015; Cullens and Thurairajah, 2021).

To illustrate the onset and end of each SSW event, we show (Figure 4) the daily variations of the zonal mean temperature and zonal wind associated with the three events of (1) 9 February 2014, (2) 26 January 2015, and (3) 8 February 2016 (mentioned by Ma Z et al., 2020b). At the onset of SSWs, the zonal mean temperature increased to over 230 K. The longitudinal area with zonal

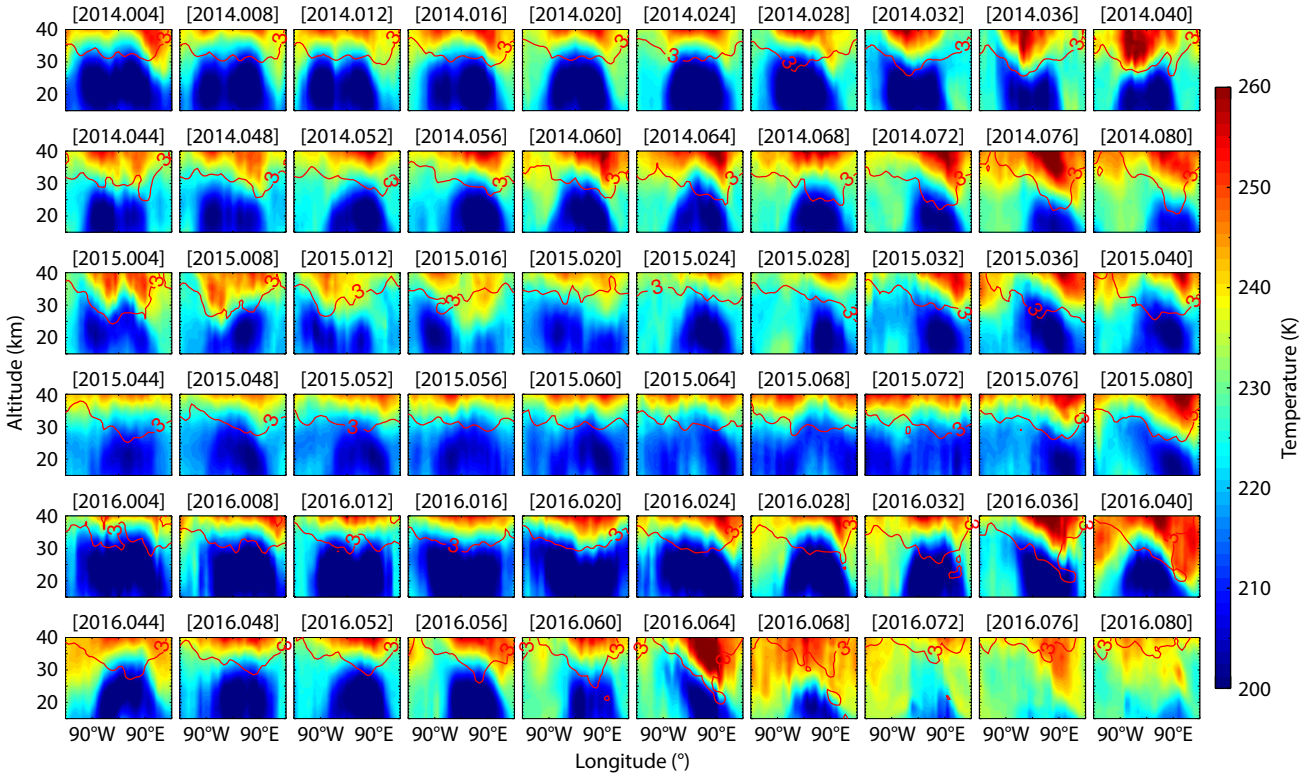

Figure 2. Longitude–altitude distribution of temperature and GW E_p at 50°N–70°N from January to March in 2014–2016 (the day of year is marked on each image; the GW E_p value of 3 J/kg is marked as the red line).

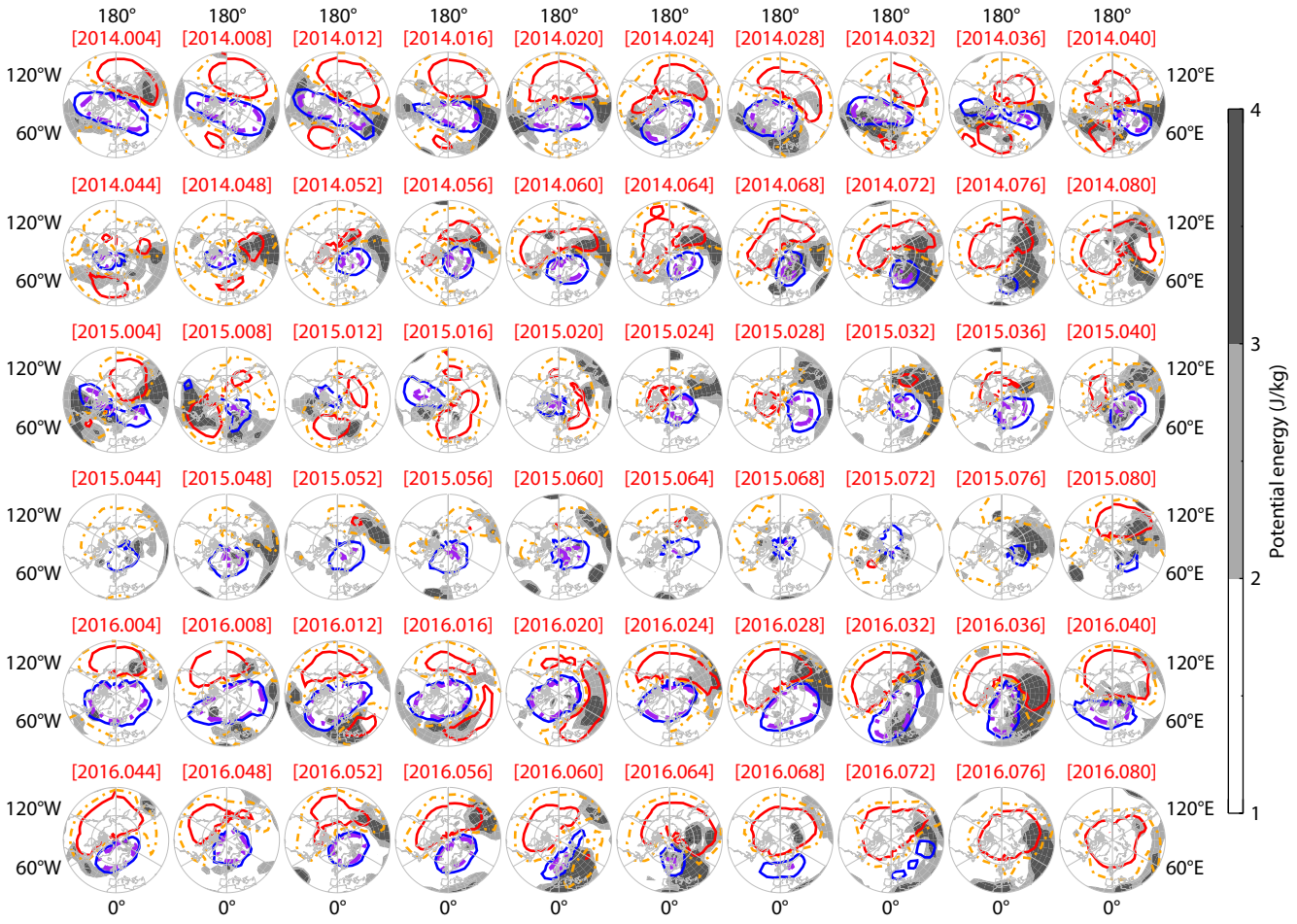

Figure 3. Longitude–latitude distribution of temperature and GW E_p at 30°N–80°N from January to March in 2014–2016 (Images are labeled as in Figure 1; the temperature values of 205, 210, 220, 225 K are marked as the purple, blue, orange, and red lines, respectively).

mean temperature higher than 220 K expanded from west of 90°W to east of 90°W. During SSWs, the E_p usually increased, while partially filtered by the westerly zonal winds. When the zonal winds weakened or turned westward, E_p began to strengthen. After SSWs, the E_p usually decreased.

Of course, vortex dynamics/type evolutions during SSWs are not in evidence in the three years from 2014 to 2016. The time period we have chosen to investigate and display did not cover all SSW events in those years, nor the complete process of each SSW event included in our study. SSWs in these three years were all minor ones, and the vortices should be the displacement type (Ma Z et al., 2020b). More work can be done in the future to analyze GW behavior during different types of SSW events.

4. Conclusions

The SSW is one of the most severe atmospheric disturbances in the winter hemisphere. The drastic changes in temperature and wind during SSWs are believed to be the main reasons for abnormal enhancement of atmospheric wave energy in the upper and middle hemispheres observed during winter. Using temperature data provided by COSMIC, we have analyzed global GW activity at 15–40 km in the Northern Hemisphere from January to March in 2014–2016, during periods when SSWs tend to occur. Our findings of the distribution and variation characteristics of temperature and GW E_p in longitude, latitude, and altitude, have been presented here and discussed. The conclusions are as follows:

(1) During warming period, the stratospheric temperature was enhanced in one or two longitudinal regions, and the heating area extended to the east of 90°W.

(2) During SSWs, the enhanced area of GW E_p expanded and covered a larger range of longitude and altitude. Significant enhancement of GW E_p was observed with an eastward and downward extension during SSWs.

(3) During SSWs, the E_p usually increased, while partially filtered by eastward zonal winds. When the zonal winds weakened or turned westward, E_p began to strengthen. After SSWs, the E_p usually decreased.

Our results can serve as a reference for future work analyzing the interaction mechanisms between SSWs and GWs. More work is needed to understand the detailed mechanisms of GW changes during SSWs and whether the changing GWs have a driving effect on SSWs. Widespread deployment of satellites and radar will provide richer observational data related to the propagation and evolution of GWs. These data can be expected to further reveal details of the excitation processes and activity patterns of GWs in the middle and upper atmosphere during SSW periods.

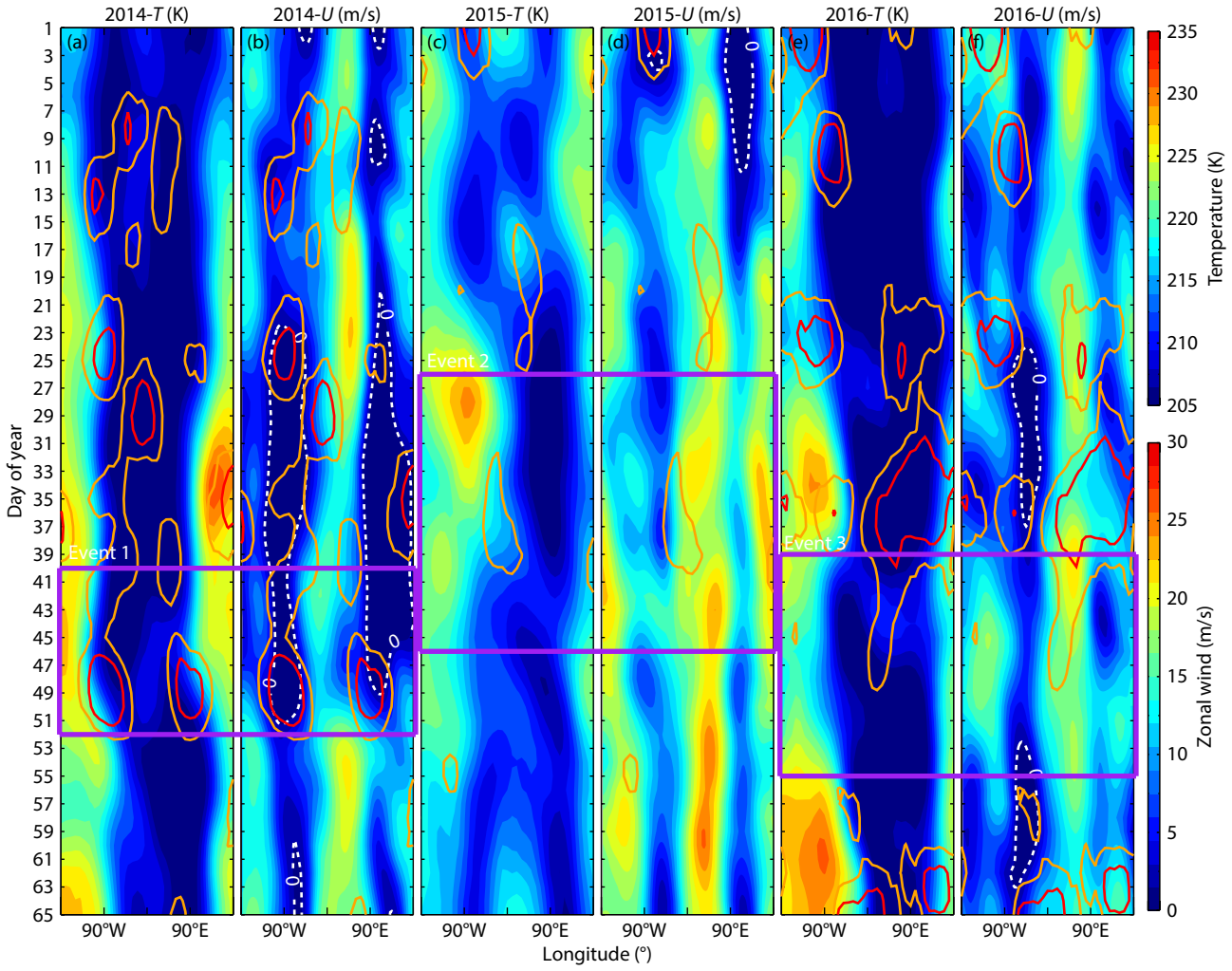

Figure 4. (a, c, e) Longitude-DOY distribution of temperature (K) at 60°N–90°N from January to March in 2014–2016; (b, d, f) the same as (a, c, e) but for zonal wind (m/s) (the values of 2.2 and 3 J/kg are marked as the orange and red solid lines, respectively; the zonal wind of 0 m/s is marked as the white dashed line).

Acknowledgments

This research was funded by the National Science Foundation of Hunan Province, China (Grant No. 2022JJ40471), the Research Foundation of the Education Bureau of Hunan Province, China (Grant No. 22B0345), and by the Key Laboratory of Geospace Environment, Chinese Academy of Sciences, University of Science & Technology of China (Grant No. GE2023-01). We acknowledge the COSMIC data used in this paper provided by the UCAR/CDAAC scientific team (http://cdaac-www.cosmic.ucar.edu/cdaac/products.html).

References

Bian, J. C., Chen, H. B., and Lu, D. R. (2005). Statistics of gravity waves in the lower stratosphere over Beijing based on high vertical resolution radiosonde. *Sci. China Ser. D Earth Sci.*, *48*(9), 1548–1558. https://doi.org/10.1360/03yd0512

Butler, A. H., and Domeisen, D. I. V. (2021). The wave geometry of final stratospheric warming events. *Weather Clim. Dynam.*, *2*(2), 453–474. https://doi.org/10.5194/wcd-2-453-2021

Chang, S. J., Sheng, Z., Ge, W., Zhang, W., He, Y., and Luo, Z. X. (2019). Intercomparison of FY-3 and AIRS gravity wave parameter extraction based on three methods. *Ann. Geophys. Discuss.*, 1–26. https://doi.org/10.5194/angeo-2019-130

Chang, S. J., Sheng, Z., Zhu, Y. W., Shi, W. L., and Luo, Z. X. (2020). Response of ozone to a gravity wave process in the UTLS region over the Tibetan Plateau. *Front. Earth Sci.*, *8*, 289. https://doi.org/10.3389/feart.2020.00289

Charlton, A. J., and Polvani, L. M. (2007). A new look at stratospheric sudden warmings. Part I: Climatology and modeling benchmarks. *J. Clim.*, *20*(3), 449–469. https://doi.org/10.1175/JCLI3996.1

Cullens, C. Y., and Thurairajah, B. (2021). Gravity wave variations and contributions to stratospheric sudden warming using long-term ERA5 model output. *J. Atmos. Solar-Terr. Phys.*, 219, 105632. https://doi.org/10.1016/j.jastp.2021.105632

Ern, M., Hoffmann, L., Rhode, S., and Preusse, P. (2022). The mesoscale gravity wave response to the 2022 tonga volcanic eruption: airs and mls satellite observations and source backtracing. *Geophys. Res. Lett.*, *49*(10), e2022GL098626. https://doi.org/10.1029/2022GL098626

Fritts, D. C., and Alexander, M. J. (2003). Gravity wave dynamics and effects in the middle atmosphere. *Rev. Geophy.*, *41*(1), 1003. https://doi.org/10.1029/2001RG000106

Ge, W., Sheng, Z., Zhang, Y. Y., Fan, Z. Q., Cao, Y., and Shi, W. L. (2019). The study of in situ wind and gravity wave determination by the first passive falling-sphere experiment in China's northwest region. *J. Atmos. Solar-Terr. Phys.*, *182*, 130–137. https://doi.org/10.1016/j.jastp.2018.11.015

Ge, W., Sheng, Z., Huang, Y. Y., He, Y., Liao, Q. X., and Chang, S. J. (2023). Different influences on "wave turbopause" exerted by 6.5 DWs and gravity

waves. *Remote Sens.*, *15*(3), 800. https://doi.org/10.3390/rs15030800

Gong, Y., Ma, Z., Lv, X. D., Zhang, S. D., Zhou, Q. H., Aponte, N., and Sulzer, M. (2018). A study on the quarterdiurnal tide in the thermosphere at Arecibo during the February 2016 sudden stratospheric warming event. *Geophys. Res. Lett.*, *45*(23), 13,142–13,149. https://doi.org/10.1029/2018GL080422

Gu, S. Y., Hou, X., Qi, J. H., TengChen K. M., and Dou, X. K. (2020). Reponses of middle atmospheric circulation to the 2009 major sudden stratospheric warming. *Earth Planet. Phys.*, *4*(5), 472–478. https://doi.org/10.26464/epp2020046

Harvey, V. L., Pierce, R. B., Fairlie, T. D., and Hitchman, M. H. (2002). A climatology of stratospheric polar vortices and anticyclones. *J. Geophys. Res.: Atmos.*, *107*(D20), 10–22. https://doi.org/10.1029/2001JD001471

He, Y., Sheng, Z., and He, M. Y. (2020a). The interaction between the turbulence and gravity wave observed in the middle stratosphere based on the round-trip intelligent sounding system. *Geophys. Res. Lett.*, *47*(15), e2020GL088837. https://doi.org/10.1029/2020GL088837

He, Y., Sheng, Z., and He, M. Y. (2020b). Spectral analysis of gravity waves from near space high-resolution Balloon data in Northwest China. *Atmos.*, *11*(2), 133. https://doi.org/10.3390/atmos11020133

He, Y., Sheng, Z., Zhang, J., He, M. Y., and Zhou, S. D. (2020c). Spectrum analysis of gravity waves based on sensors mounted on a new round-trip airborne flat-floating sounding system. *Sensors*, *20*(7), 2123. https://doi.org/10.3390/s20072123

He, Y., Sheng, Z., Zhou, L. S., He, M. Y., and Zhou, S. D. (2020d). Statistical analysis of turbulence characteristics over the tropical western pacific based on radiosonde data. *Atmos.*, *11*(4), 386. https://doi.org/10.3390/atmos11040386

He, Y., Zhu, X. Q., Sheng, Z., Zhang, J., Zhou, L. S., and He, M. Y. (2021). Statistical characteristics of inertial gravity waves over a tropical station in the western Pacific Based on high-resolution GPS radiosonde soundings. *J. Geophys. Res.-Atmos.*, *126*(11), e2021JD034719. https://doi.org/10.1029/2021JD034719

He, Y., Zhu, X., Sheng, Z., He, M., and Feng, Y. (2022a). Observations of inertia gravity waves in the western pacific and their characteristic in the 2015/2016 quasi-biennial oscillation disruption. *J. Geophys. Res.: Atmos.*, *127*(22), e2022JD037208. https://doi.org/10.1029/2022JD037208

He, Y., Zhu, X. Q., Sheng, Z., Ge, W., Zhao, X. R., and He, M. Y. (2022b). Atmospheric disturbance characteristics in the lower-middle stratosphere inferred from observations by the Round-Trip Intelligent Sounding System (RTISS) in China. *Adv. Atmos. Sci.*, *39*, 131–144. https://doi.org/10.1007/s00376-021-1110-2

He, Y., Zhu, X. Q., Sheng, Z., and He, M. Y. (2023). Identification of stratospheric disturbance information in China based on round-trip intelligent sounding system. *EGUsphere*, *2023*(2023), 1–23 https://doi.org/10.5194/egusphere-2023-1608

Idolor, O. R., Akala, A. O., and Bolaji, O. S. (2021). Responses of the African and American equatorial ionization anomaly (EIA) to 2014 arctic SSW events. *Space Weather*, *19*(11), e2021SW002812. https://doi.org/10.1029/2021SW002812

Ji, Q. Q., Zhu, X. Q., Sheng, Z., and Tian, T. Spectral analysis of gravity waves in the martian thermosphere during low solar activity based on MAVEN/NGIMS observations. *Astrophys. J.*, 2022, 938(2): 97. https://doi.org/10.3847/1538-4357/ac8d07

Jia, M. J., Xue, X. H., Gu, S. Y., Chen, T. D., Ning, B. Q., Wu, J. F., Zeng, X. Y., Dou, X. K. (2018). Multiyear observations of gravity wave momentum fluxes in the midlatitude mesosphere and lower thermosphere region by meteor radar. *J. Geophys. Res.: Space Phys.*, *123*(7), 5684–5703. https://doi.org/10.1029/2018JA025285

Jia, Y., Zhang, S. D., Yi, F., Huang, C. M., Huang, K. M., Gan, Q., and Gong, Y. (2015). Observations of gravity wave activity during stratospheric sudden warmings in the Northern Hemisphere. *Sci. Chin. Tech. Sci.*, *58*(6), 951–960. https://doi.org/10.1007/s11431-015-5806-3

Jin, S. G., Dam, T. V., and Wdowinski, S. (2013). Observing and understanding the Earth system variations from space geodesy. *J. Geodyn.*, *72*(12), 1–10. https://doi.org/10.1016/j.jog.2013.08.001

Jin, S. G., Feng, G. P., and Gleason S. (2011). Remote sensing using GNSS signals: Current status and future directions. *Adv. Space Res.*, *47*(10), 1645–1653. https://doi.org/10.1016/j.asr.2011.01.036

Kalisch, S., and Chun, H. Y. (2021). AIRS satellite observations of gravity waves during the 2009 sudden stratospheric warming event. *J. Geophys. Res.: Atmos.*, *126*(4), e2020JD034073. https://doi.org/10.1029/2020JD034073

Kogure, M., Yue, J., and Liu, H. X. (2021). Gravity wave weakening during the 2019 Antarctic stratospheric sudden warming. *Geophys. Res. Lett.*, *48*(8), e2021GL092537. https://doi.org/10.1002/essoar.10505858.2

Laskar, F. I., McCormack, J. P., Chau, J. L., Pallamraju, D., Hoffmann, P., and Singh, R. P. (2019). Interhemispheric meridional circulation during sudden stratospheric warming. *J. Geophys. Res.: Space Phys.*, *124*(8), 7112–7122. https://doi.org/10.1029/2018JA026424

Li, T., She, C. Y., Liu, H. L., and Michael, T. M. (2007). Evidence of a gravity wave breaking event and the estimation of the wave characteristics from sodium lidar observation over Fort Collins, CO (41°N, 105°W). *Geophys. Res. Lett.*, *34*(5), L05815. https://doi.org/10.1029/2006GL028988

Ma, Z., Gong, Y., Zhang, S. D., Luo, J. H., Zhou, Q. H., Huang, C. M., and Huang, K. M. (2020a). Comparison of stratospheric evolution during the major sudden stratospheric warming events in 2018 and 2019. *Earth Planet. Phys.*, *4*(5), 493–503. https://doi.org/10.26464/epp2020044

Ma, Z., Gong, Y., Zhang, S. D., Zhou, Q. H., Huang, C. M., Huang, K. M., Luo, J. H., Yu, Y., and Li, G. Z. (2020b). Study of a quasi 4-day oscillation during the 2018/2019 SSW over Mohe, China. *J. Geophys. Res.: Space Phys.*, *125*(7), e2019JA027687. https://doi.org/10.1029/2019JA027687

Manney, G. L., Lawrence, Z. D., Santee, M. L., Read, W. G., Livesey, N. J., Lambert, A., Froidevaux, L., Pumphrey, H.C., and Schwartz, M. J. (2015). A minor sudden stratospheric warming with a major impact: Transport and polar processing in the 2014/2015 Arctic winter. *Geophys. Res. Lett.*, *42*(18), 7808–7816. https://doi.org/10.1002/2015GL065864

Mcdonald, A. J. (2012). Gravity wave occurrence statistics derived from paired COSMIC/FORMOSAT3 observations. *J. Geophys. Res.: Atmos., 117*(D15). https://doi.org/10.1029/2011jd016715

Minamihara, Y., Sato, K., and Watanabe, S. (2022). Dynamical Characteristics of Quasi-6-day Rossby Waves and Gravity Waves during the Stratospheric Sudden Warming in the Southern Hemisphere in 2019 (Authorea Preprints) https://doi.org/10.1002/essoar.10511060.1

Scherhag R. (1952). Die explosionsartigen Stratosphärenerwärmungen des Spätwinters 1951/52. *Berichte des Deutschen Wetterdienstes in der US-Zone, 6*(38), 51–63.

Seviour, W. J. M., Mitchell, D. M., and Gray, L. J. (2013). A practical method to identify displaced and split stratospheric polar vortex events. *Geophys. Res. Lett.*, *40*(19), 5268–5273. https://doi.org/10.1002/grl.50927

Tang, L., Gu, S. Y., Teng, C. K. M., Yang, Z. L., Zhao, S. Y., Huang, H., and Wang, D. (2023). On the different quasi-2-Day wave behaviors during sudden stratospheric warming periods. *Atmos.*, *14*(3), 521. https://doi.org/10.3390/atmos14030521

TengChen, K. M., Gu, S. Y., Qin, Y., Dou, X., Li, N., and Tang, L. (2021). Unexpected decrease in TW3 amplitude during antarctic sudden stratospheric warming events as revealed by SD-WACCM-X. *J. Geophys. Res.: Space Phys.*, *126*(10), e2020JA029050. https://doi.org/10.1029/2020JA029050

Tsuda, T., and Noersomadi. (2016). Global distribution of vertical wavenumber spectra in the lower stratosphere observed using high-vertical-resolution temperature profiles from cosmic gps radio occultation. *Ann. Geophys.*, *34*(2), 203–213. https://doi.org/10.5194/angeo-34-203-2016

Wang, L., and Alexander, M. J. (2009). Gravity wave activity during stratospheric sudden warmings in the 2007–2008 Northern Hemi-sphere winter. *J. Geophys. Res.: Atmos., 114*(D18), D18108. doi:10.1029/2009JD011867

Watanabe, S., Koshin, D., Noguchi, S., and Sato, K. (2022). Gravity wave morphology during the 2018 sudden stratospheric warming simulated by a whole neutral atmosphere general circulation model. *J. Geophys. Res.: Atmos.*, *127*(19), e2022JD036718 https://doi.org/10.1029/2022JD036718

Wicker, W., Polichtchouk, I., and Domeisen, D. I. V. (2023). Increased vertical resolution in the stratosphere reveals role of gravity waves after sudden stratospheric warmings. *Weather Clim. Dynam.*, *4*(1), 81–93. https://doi.org/10.5194/wcd-4-81-2023

Wright, C. J., Rivas, M. B., and Gille, J. C. (2011). Intercomparisons of HIRDLS, COSMIC and SABER for the detection of stratospheric gravity waves. *Atmos. Meas. Tech. Discuss.*, *4*(1), 1581–1591. https://doi.org/10.5194/amtd-4-737-2011

Wu, D. L., and Waters, J. W. (1996). Gravity-wave-scale temperature fluctuations seen by the UARS MLS. *Geophys. Res. Lett.*, *23*(23), 3289–3292. https://doi.org/10.1029/96GL02924

Wu, J. F., Xue, X. H., Liu H. L., Dou X. K., and Chen, T. D. (2018). Assessment of the simulation of gravity waves generation by a tropical cyclone in the high-resolution waccm and the wrf. *J. Adv. Model. Earth Sy.*, *10*(9), 2214–2227. https://doi.org/10.1029/2018MS001314

Wu, Y., Sheng, Z., and Zuo, X. J. (2022). Application of deep learning to estimate stratospheric gravity wave potential energy. *Earth Planet. Phys.*, *6*(1), 70–82. https://doi.org/10.26464/epp2022002

Xiao, C. Y., and Hu, X. (2010). Analysis on the global morphology of stratospheric gravity wave activity deduced from the COSMIC GPS occultation profiles. *GPS Sol.*, *14*(1), 65–74. https://doi.org/10.1007/s10291-009-0146-z

Xue, X. H., Sun, D. S., Xia, H. Y., and Dou, X. K. (2020). Inertial gravity waves observed by a Doppler wind LiDAR and their possible sources. *Earth Planet. Phys.*, *4*(5), 461–471. https://doi.org/10.26464/epp2020039

Yamazaki, Y., and Matthias, V. (2019). Large-amplitude quasi-10-day waves in the middle atmosphere during final warmings. *J. Geophys. Res.: Atmos.*, *124*(17-18), 9874–9892. https://doi.org/10.1029/2019JD030634

Yi, W., Xue, X. H., Chen, J. S., Chen, T. D., and Li, N. (2019). Quasi-90-day oscillation observed in the MLT region at low latitudes from the Kunming meteor radar and SABER. *Earth Planet. Phys.*, *3*(2), 136–146. https://doi.org/10.26464/epp2019013

Yi, W., Xue, X. H., Reid, I. M., Murphy, D. J., Hall, C. M., Tsutsumi, M., Ning, B. Q., Li, G. Z., Yang, G. T., Li, N., Chen, T. D., and Dou, X. K. (2021). Climatology of interhemispheric mesopause temperatures using the high-latitude and middle-latitude meteor radars. *J. Geophys. Res.: Atmos.*, *126*(6), e2020JD034301. https://doi.org/10.1029/2020JD034301

Yi, W., Xue, X. K., Zeng, J., Wang, J. Y., Zhou, B. Z., Ye, H. L., Chen T. D., and Dou, X. K. (2023). Observation of MLT region winds and tides by the USTC Mengcheng meteor radar. *JUSTC*, *53*(5), 0501–1. https://doi.org/10.52396/JUSTC-2022-0158

Yi, W., Xue, X. H., Lu, M. L., Zeng, J., Ye, H. L., Wu, J. F., Wang, C., and Chen, T. D. (2023). Mesopause temperatures and relative densities at midlatitudes observed by the Mengcheng meteor radar. *Earth Planet. Phys.*, *7*(6), 1–10. https://doi.org/10.26464/epp2023083

Zeng, X. Y., Xue, X. H., Dou, X. K., Liang, C., and Jia, M. J. (2017). COSMIC GPS observations of topographic gravity waves in the stratosphere around the Tibetan Plateau. *Sci. Chin. Earth Sci.*, *60*(1), 188–197. https://doi.org/10.1007/s11430-016-0065-6

Zeng, X. Y., Peng, Y., and Liu, S. (2021). Three-dimensional analysis of global gravity waves based on COSMIC multi-satellite observations. *Geophys. Res. Lett.*, *48*(20), e2021GL094809. https://doi.org/10.1029/2021GL094809

Zhang, J., Ji, Q. Q., Sheng, Z., He, M. Y., He, Y., Zuo, X. J., He, Z. F., Qin, Z. L., and Wu, G. Y. (2023). Observation based climatology Martian atmospheric waves perturbation Datasets. *Sci. Data*, 10(4). doi:10.1038/s41597-022-01909-y

Zhou, B. Z., Yi, W., Xue, X. H., Ye, H. L., Zeng, J., Li, G. Z., Masaki, T., Njål, G., Chen, T. D., and Dou, X. K. (2023). Impact of sudden stratospheric warmings on the neutral density, temperature and wind in the MLT region. *Front. Astron. Space Sci.*, *10*, 1192985. https://doi.org/10.3389/fspas.2023.1192985